Non-linear viscoelastic performance of Nomex, Kevlar and polypropylene fibres in a single-step stress relaxation test: 1. Experimental data and principles of analysis

F.-J. Wortmann* and K. V. Schulz
Deutsches Wollforschungsinstitut, Veltmanplatz 8, D-51 Aachen, Germany
(Received 8 March 1993; revised 14 June 1993)

This study, summarized in two parts, is directed at the investigation of the non-linear performance of Nomex, Kevlar and polypropylene fibres, when undergoing stress relaxation tests. The description of the strain-dependent performance is based on a two-component model, which comprises an elastic and a viscous contribution. A shape-invariant relaxation function is introduced that is based on the cumulative log-normal distribution. This first part is directed at the description of the experimental procedures and of the approach to the analysis of the stress relaxation data.

(Keywords: stress relaxation; non-linear viscoelasticity; fibres)

INTRODUCTION

The theory of linear viscoelasticity (LVE) for polymers is, similarly to Hooke's law for elastic materials, only an approximation of the real material performance. Linear viscoelasticity is generally assessed by checking the applicability of the criteria of proportionality and of superposition in one of two simple experiments, namely isothermal stress relaxation or creep (e.g. ref. 1).

The range of linear viscoelasticity, extending for glassy polymers over comparatively small stresses and strains[2], is generally the range for the application of polymers as engineering materials, where the calculation of the mechanical performance of structures can be conducted with a high degree of accuracy[2,3]. Strains outside the range of LVE, i.e. beyond ca. 1% for amorphous and 0.4% for semicrystalline, glassy polymers[2], are considered as critical for engineering applications[3], since the region of non-linear viscoelasticity borders on that of material failure.

To further the understanding of the role of strain for the non-linear viscoelastic (NLVE) performance of polymers, this study, summarized in two parts[4], is directed at the investigation of the strain-induced NLVE effects in Nomex®, Kevlar® and polypropylene fibres, when undergoing a single-step stress relaxation test. These polymers were specifically chosen as examples of materials exhibiting typical types of mechanical behaviour, as expressed by their stress–strain curves (see *Figure 1*), as well as for their technical and economic relevance.

An analytical model is introduced that enables us to describe systematically the strain-dependent stress relaxation performance of the three types of polymer fibres. The analysis is based on a two-component model, as implied in the theory of linear viscoelasticity[5], which comprises an elastic component and a viscoelastic contribution, the time dependence of which is described by a shape-invariant relaxation function. The application of the model to stress relaxation data leads to the detection of pronounced strain-induced modulus changes of the components and of a shift of the relaxation function with strain that is consistent with a solid–fluid transition.

This first of two papers is directed at the description of the experimental procedures, the approach to the analysis of the resulting data and the assessment of the performance of the analysis procedure. The second part[4] is directed at the discussion of the implications of the results with respect to the morphology of the materials and to their rheological performance.

MATERIALS

Kevlar (poly(*p*-phenylene terephthalamide)), investigated in the form of Kevlar 29 (DuPont), is a fibre with a high degree of orientation and crystallinity that is spun from a liquid-crystalline solution of extended-chain molecules. The ensuing structure of parallel, densely packed chain molecules is assumed to be only disturbed by chemical 'defects', introduced by chain ends, and by structural defects, like kinks and dislocations[6]. In consequence, Kevlar is an example of a highly elastic polymeric fibre with a high elastic modulus and a low breaking strain (see *Table 1* and *Figure 1*).

Though the chemical structure of Nomex (poly(*m*-phenylene isophthalamide)) is somewhat similar to that

* To whom correspondence should be addressed

0032-3861/94/10/2108–09

Table 1 Values of the initial modulus, E, the breaking stress, σ_B, and the breaking strain, ε_B, of the Kevlar, Nomex and polypropylene (PP) fibres used in this study, determined from a minimum of 15 fibres according to ASTM D2101[11]

Fibre type	E (GPa)	σ_B (MPa)	ε_B (%)	A (μm^2)	$\Delta\varepsilon$ (%)
Kevlar $\bar{x}$	73.3	2450	2.9	115	0.139
CV(%)	11	26	25	10	
Nomex $\bar{x}$	13.7	502	34	170	0.144
CV(%)	13	4	18	7	
PP $\bar{x}$	1.65	258	151	365	0.023 (n.s.)
CV(%)	13	6	15	17	

$\Delta\varepsilon$ is the correction term for the calculation of true fibre strain; (n.s.) denotes statistically 'not significant' at the 90% significance level. A is the fibre cross-sectional area, determined by the vibroscope method, $\bar{x}$ is the arithmetic mean and CV the coefficient of variation

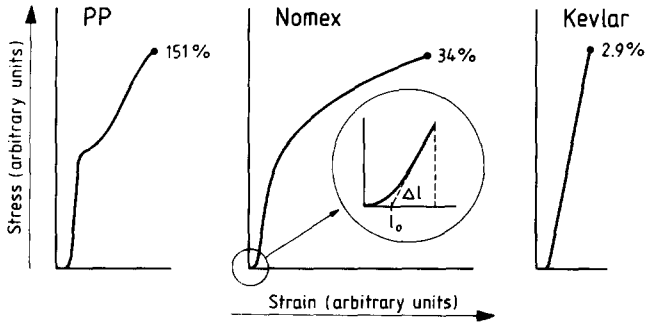

Figure 1 Qualitative comparison of the stress–strain curves of polypropylene (PP), Nomex and Kevlar fibres. To facilitate the comparison, the mean fracture strain is given for each case. The inset for the Nomex curve elucidates the concept of initial fibre length l_0 and length change Δl

of Kevlar, the *meta* links of the monomeric unit introduce kinks into the polymer backbone[7] and thus hinder a high degree of structural organization. In consequence, Nomex shows the stress–strain behaviour typical for a partially crystalline, glassy polymer and similar to that of aliphatic polyamides. Compared to Kevlar, Nomex has a 5–6 times lower modulus (see *Table 1*) and shows beyond ca. 2% strain an extended yield region (see *Figure 1*) up to the breaking point around 35% strain. With a high glass transition temperature of $T_g \simeq 350°C$[6], due to the highly aromatic polymer backbone, at around room temperature Nomex is far within the glassy region of mechanical behaviour.

The polypropylene (PP) fibres that were examined are a commercial, isotactic product for textile purposes (Vestolen P1200, Chem. Werke Hüls AG). Isotactic polypropylene is a thermoplastic, partially crystalline ($\simeq 60\%$) hydrocarbon polymer, for which the glass transition temperature $T_g \simeq -10°C$ is well below room temperature[8]. The modulus of polypropylene is approximately one order of magnitude smaller than that for Nomex (see *Table 1*) and the fibre exhibits, beyond $\simeq 10\%$ strain, a very extended yield region up to the breaking strain around 150% (see *Figure 1*).

With respect to their chemistry, structures, glass transition temperatures and stress–strain curves, the three types of fibres represent a wide range of polymer performance, for which, on extending a previous account of some of the data[9], a systematic and uniform description of the NLVE stress relaxation behaviour is sought.

EXPERIMENTAL

The single-step stress relaxation test, as schematically described in *Figure 2*, is one of the simplest methods for the examination of the viscoelastic properties of polymer fibres. The fibre is deformed within a short period of time, Δt, to a predetermined strain, ε, at a constant rate of deformation, $\dot{\varepsilon} = \varepsilon/\Delta t$ (e.g. 20%/min). Subsequently the strain is held constant and the drop of the resulting force F is followed with time, where the starting point of the relaxation and hence the start of the experimental timescale is the end-point of the straining step, t_0. $F(0)$ is the initial force and $F_\infty \equiv F(\infty)$ the generally unknown value for the equilibrium force for $t \to \infty$.

The relaxation modulus, $E(t)$, for a given initial fibre cross-section, A, is given, corresponding to the elastic case, by:

$$E(t) = F(t)/(A\varepsilon) \quad (1)$$

where the strain, irrespective of strain level, is given by:

$$\varepsilon = \Delta l/l_0 \quad (2)$$

Δl is the length change and l_0 is the initial specimen length, determined according to the procedure described in the following section and illustrated by the inset in *Figure 1*.

To minimize influences due to relaxation during the strain step and due to experimental background effects, which become significant at longer experimental times, only data in the range $\Delta t < t < 10^4$ s were used for the analysis.

Prior to the stress relaxation experiments, the cross-sectional areas of the individual fibres were determined with a vibroscope (Fa. Insco). The mean cross-sectional areas of the fibres are given in *Table 1*.

All experiments were conducted on an Instron (Type 1122) tensile testing machine in a room of standard climatic conditions (22°C, 65% r.h.). To minimize influences of thermal fluctuations, the specimen and its clamping arrangement were enclosed in a glass cylinder for which a temperature-controlled water jacket ensured a constancy of the temperature within less than $\pm 0.5°C$ during the experiment. At the bottom of the cylinder a layer of an appropriate glycerol/water mixture ensured furthermore a stable relative humidity (65% r.h.) around the specimen.

To increase the force signal and to facilitate fibre alignment, the fibres were examined in the form of loops

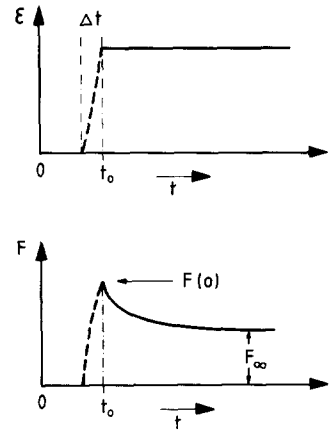

Figure 2 Strain (ε) and force (F) changes, schematically, during a single-step stress relaxation test

of 50 mm overall length that were led over a stainless-steel hook (1.5 mm diameter) connected to the load cell. The ends of the loop were secured by an appropriate clamping arrangement to the moving cross-head of the machine[10]. The results in *Table 1* were obtained with this set-up and applying the principles of ASTM D2101[11].

Machine characteristics, like baseline drift at low stresses and machine deformations at high stresses, were determined prior to the experiments. They were found to be negligible for most of the experimental range and were corrected when necessary. The influence tolerated by such effects without correction was set to 0.1% relative to the force signal.

Strain correction

When performing stress–strain tests on fibres it is a common phenomenon that the resulting curves exhibit a more or less pronounced curved region at low stresses, attributable to fibre decrimping and geometrical alignment of the experimental set-up. As outlined in ASTM D2101[11] and illustrated in the enlarged inset of the Nomex curve in *Figure 1*, this effect is corrected for by extrapolating the linear part of the force–elongation curve to zero force, and thus determining the effective specimen length, l_0, with respect to the original separation of the fixation points of the fibre loop.

The clamping arrangement for gripping the fibre ends consisted of flat jaws, the faces of which were plated with combinations of Teflon, aluminium and rubber, individually chosen for a fibre type to minimize slippage. Gross fibre slippage, whether continuous or discontinuous, is usually readily detectable in the force–elongation curves. However, to show the nature and size of less obvious effects, *Figure 3* summarizes strain *versus* initial stress results, that is ε *versus* $\sigma(0)=F(0)/A$, for the three types of fibres for low strains ($\varepsilon<2\%$). Regression analysis shows that the strain data follow straight lines ($r^2 \geqslant 0.95$ in all cases) that intersect with the y-axis at positive strains, which are statistically significant (90% confidence limits) for Kevlar and Nomex (see *Table 1*). In consequence, all experimentally determined strains were corrected individually for each fibre type by subtracting the values of $\Delta\varepsilon$, given by the positive y-axis intercepts of the regression (see *Table 1*).

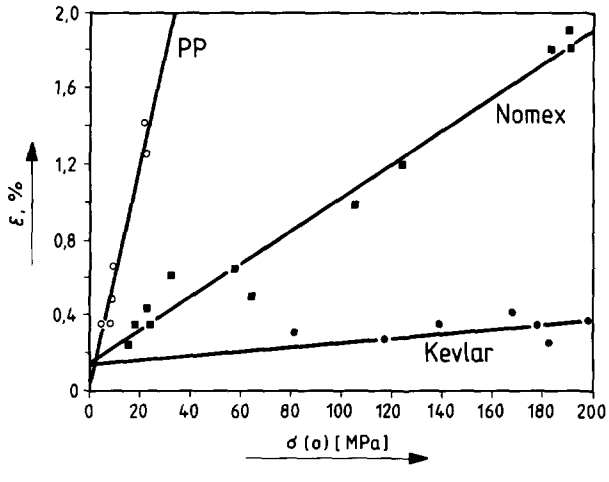

Figure 3 Initial stress $\sigma(0)$ and strain ε for the region of low strains ($\varepsilon<2\%$). Data points from individual experiments are given for the three types of fibres. Full lines are linear regression lines

APPROACH TO NON-LINEAR VISCOELASTICITY

The conventional description for the viscoelastic behaviour of polymers in stress relaxation is given by[5]:

$$E(t)=E_\infty+\Delta E\Psi(t) \tag{3}$$

This approach comprises two components: a time-independent, elastic component, E_∞; and a viscous component with a limiting elastic modulus, $\Delta E=(E_0-E_\infty)$, where E_0 is the upper limiting modulus. The time dependence of the properties of the viscous component is described by the relaxation function, $\Psi(t)$, formally given by:

$$\Psi(t)=\int_{-\infty}^{+\infty} h(\tau)\,e^{-t/\tau}\,d\ln\tau \tag{4}$$

where $h(\tau)$ is the normalized relaxation-time spectrum with the property:

$$\int_{-\infty}^{+\infty} h(\tau)\,d\ln\tau=1 \tag{5}$$

In parallel to the widespread use of the expanded exponential form of the Kohlrausch–Williams–Watts (KWW) function, a certain tradition has been established in keratin research to describe the stress relaxation function using the log-normal or rather the cumulative log-normal distribution (CLND) function given for the $\log_{10}$(time) scale by:

$$\Psi(t)=[1/(\sqrt{2\pi}\beta)]\int_{\log t}^{\infty}\exp\{-\tfrac{1}{2}[(x-\alpha)/\beta]^2\}\,dx \tag{6}$$

where α is the mean and β the standard deviation of the underlying log-normal distribution, which, on the basis of Alfrey's rule[12], is an approximation of the distribution of relaxation times, as suggested by Feltham[13] and as originally introduced by Wiechert[14]. On the basis of this description $\Psi(t)$ forms a strictly symmetrical S-shaped curve on the log(time) scale, which drops from unity to zero within a range of approximately $\alpha\pm4\beta$.

The model described by equations (3) and (6) will be referred to as the two-component (TC) model, in what follows, which is a more general term for the two-phase model successfully applied by the authors for the interpretation of the thermorheological and hydrorheological properties of semicrystalline, biological and synthetic polymers[9,15–17]. The general procedure to fit the model to the data is described in the Appendix.

The application of equations (3) and (4) or rather of equations (3) and (6) as a basis for the analysis of relaxation data implies that, during the time interval to be studied, the relaxation functions are invariant, meaning on a more general scale that the material is non-ageing according to the principles outlined by Struik[18]. This assumption is justified in view of the experimental time of ca. 2 h being very small compared to the storage time and hence the ageing time for the commercial materials of at least several months prior to the tests.

Furthermore, equation (3) is a valid description of the relaxation behaviour only in the LVE region, which even for glassy amorphous polymers extends only to a maximum of 1% strain[2]. To extend this approach for non-linear viscoelastic properties, induced by strains beyond this limit, an extension of equation (3) based on Schapery's theory[19] is used as:

$$E(t,\varepsilon)=h_e(\varepsilon)E_\infty^R+h_v(\varepsilon)\Delta E^R\Psi(t/a(\varepsilon)) \tag{7}$$

Here E_∞^R and ΔE^R are the moduli of the elastic and the viscoelastic components at a reference strain within the LVE range; h_e and h_v are the strain functions that describe the changes of the reference moduli of the elastic and viscoelastic components, respectively. The strain-induced shift of the relaxation function on a log(time) scale with respect to the reference state is described by the acceleration factor, $a(\varepsilon)$. From a thermodynamic point of view, the strain-dependent properties of h_e and h_v are due to third- and higher-order strain effects in the Helmholtz free energy, while changes in $a(\varepsilon)$ arise from strong strain influences in both entropy production and free energy[19].

On the basis of the description of the relaxation function in equation (6), the acceleration factor $a(\varepsilon)$ in equation (7) is given by:

$$\log a(\varepsilon) = \alpha(\varepsilon) - \alpha(\varepsilon^R) \quad (8)$$

where $\alpha(\varepsilon)$ and $\alpha(\varepsilon^R)$ are the mean log-relaxation times at a given strain, ε, and at the chosen reference strain, ε^R, respectively. This description assumes strain invariance of the shape of the relaxation function, which, translated into the physical model, implies invariant strain activation for all relaxation times. This is in contrast to the hypothesis of a narrowing of the relaxation-time spectrum with strain[20], as backed by experiments on polycarbonate[21].

It is not by chance that equation (7) is similar to Schapery's[19] description of generally thermorheologically complex materials, thus implying, quite generally, an equivalence between the effects of strain and of temperature, namely the yield of polymers is often treated as a transition from solid-like to fluid-like behaviour, much like a thermally induced solid–fluid transition[21–23].

Equation (7) comprises a number of simpler models that relate to superposition of the curves by horizontal and/or vertical shifts on the log E *versus* log t scale, and which with respect to their applicability for the cases presented here will be discussed in part 2[4].

CHOOSING THE SHAPE OF THE RELAXATION FUNCTION

Figures 4–6 summarize experimental data for the relaxation stress of Nomex, Kevlar and polypropylene fibres for various strains and in the conventional double-logarithmic plot. For each material the data follow,

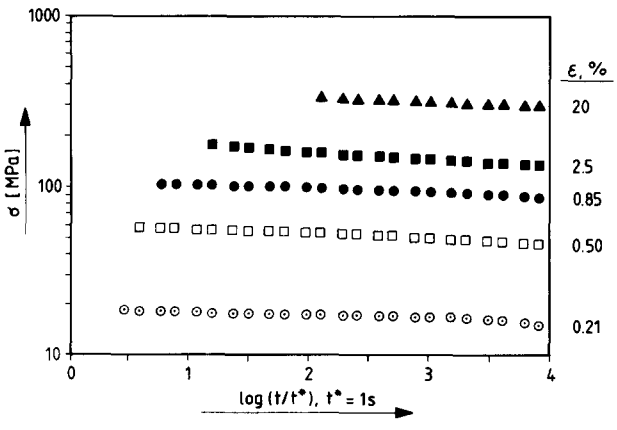

Figure 4 Stress relaxation data, $\sigma(t)$, for Nomex fibres at the strain levels (%) indicated

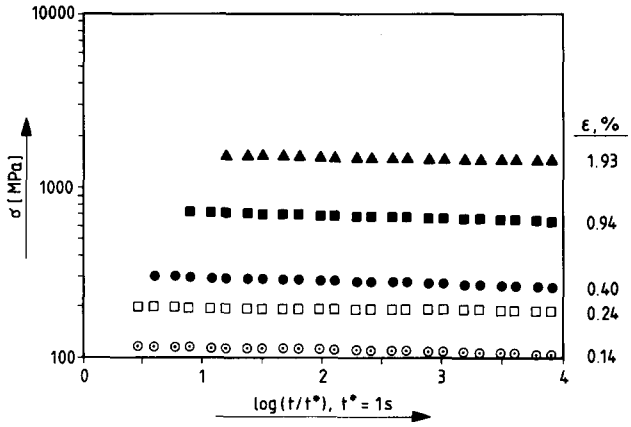

Figure 5 Stress relaxation data, $\sigma(t)$, for Kevlar fibres at the strain levels (%) indicated

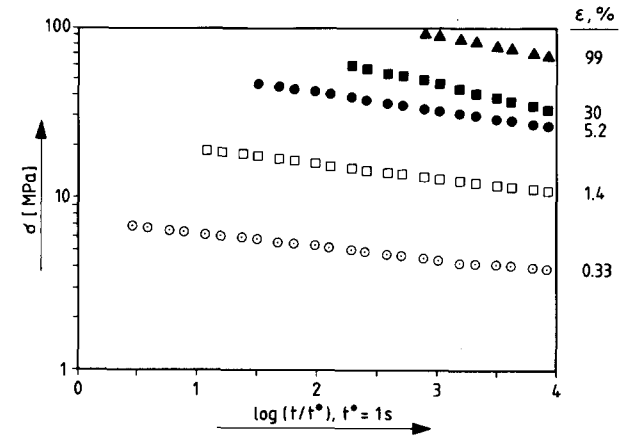

Figure 6 Stress relaxation data, $\sigma(t)$, for polypropylene fibres at the strain levels (%) indicated

irrespective of strain magnitude, virtually straight lines of similar, if not equal slope, where the decision for a horizontal and/or vertical shift, and hence for the interpretation based thereon, would be difficult to make.

Investigations by the authors into the properties of the generalized TC model, represented by equations (6) and (7), have shown[10,24] that it is generally not trivial to obtain a stable fit of the model to the experimental data in *Figures 4–6*. Within the restrictions imposed by the experimentally accessible time range of up to 10^4 s, the fits generally become unstable towards increasing E_0 and decreasing E_∞. This effect is documented by the surface contour plot in *Figure 7*, showing levels of equal goodness of fit on the $E_0/E(0)$ *versus* $E_\infty/E(0)$ plane (see Appendix) for an experimental relaxation curve of a Nomex fibre ($\varepsilon = 1\%$). Though the chosen case is atypical, in that it deviates in its performance markedly from other similar measurements, it was chosen for illustrative purposes owing to the significant offset of the minimum along both axes. However, rather than showing a well defined minimum, the lowest contour line for $(1 - r^2) \times 10^4$, as the parameter to be minimized (see Appendix), encloses a very 'shallow valley' that opens continuously to slightly lower minima towards the lower right corner of the surface and beyond.

Restrictions to stabilize the fit may be introduced by applying assumptions that lead to a superposition of the curves by rigid horizontal and/or vertical shifts on a log E *versus* log t scale. However, an alternative restriction may

be introduced by using an *a priori* assumption about the shape of the relaxation function, namely of the value of the standard deviation β in equation (6). A detailed discussion of alternative models to systematize the data is presented in part 2[4].

The choice of the value of β is based on Kubat's work[25,26] on the material invariance of the shape of the relaxation function for different polymers and metals. An analysis of Kubat's data showed that the width of the relaxation function for the materials may be well described on the $\log_{10}$(time) scale by using a value for the standard deviation in the CLND function in the range of $\beta = 2$[9,16,17,27]. Following the initial observation of this phenomenon[27], a value of $\beta = 1.9_0$ was chosen for the current investigation.

Extending a previous account of the analysis[27], data for the relaxation stress, $\sigma(t)$, for indium, cadmium, lead, Lipowitz alloy, rubber hydrochloride, polyisobutylene, polyethylene and cetyl alcohol were calculated from the values given by Kubat[25,26] for initial stress $\sigma(0)$, for relative equilibrium stress $\sigma_\infty/\sigma(0)$ and for the relaxation function. Subsequently the TC model was fitted to the data on the basis of $\beta = 1.9_0$, by applying the procedure described in the Appendix. Kubat's estimates for $\sigma(0)$ and for $\sigma_\infty/\sigma(0)$ and the results of the optimization/fitting procedure are summarized in *Table 2*. The quality of the fits of the relaxation function data onto a common master curve is documented in *Figure 8*, where $\Psi(t)$ is plotted for the eight materials *versus* the standardized time parameter, u. The shape of the relaxation function is consistent with Kubat's observation for the ln(time) scale that the slope at the turnover point is material-invariant as 0.1 ± 0.01[25]. The value calculated on the basis of equation (6) and $\beta = 1.9_0$ is $d\Psi/d \ln t|_{\alpha \ln 10} = 0.091$.

The results in *Table 2* show, in accordance with the results summarized in *Figure 8*, that the quality of the fits is rather satisfactory in all cases ($r^2 > 0.98$). Values of $r^2 < 0.99$ relate in all cases to systematic differences between experiment and theory in the region of low values of $\Psi(t)$ ($\lesssim 0.15$), where the deviations may be attributed to generally unknown background effects, which may, for example, relate to a further long-term relaxation process.

The deviations in the estimates of initial stress may be attributed to the restriction in this analysis to data for $t > \Delta t$, in order to suppress most effects of relaxation

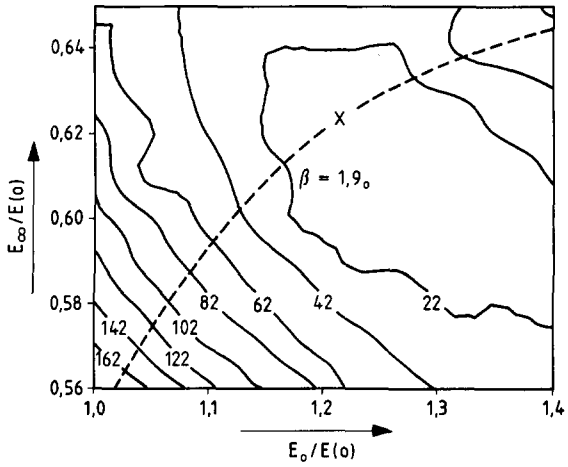

Figure 7 Contour plot for the coefficient of non-determination $(1-r^2) \times 10^4$ in the $E_0/E(0)$ vs. $E_\infty/E(0)$ plane, when fitting the CLND function to experimental data for the relaxation curve of a Nomex fibre at 1% strain. The broken curve through the plot connects the cases of a constant standard deviation of $\beta = 1.9_0$. The cross (×) marks the minimum along the line

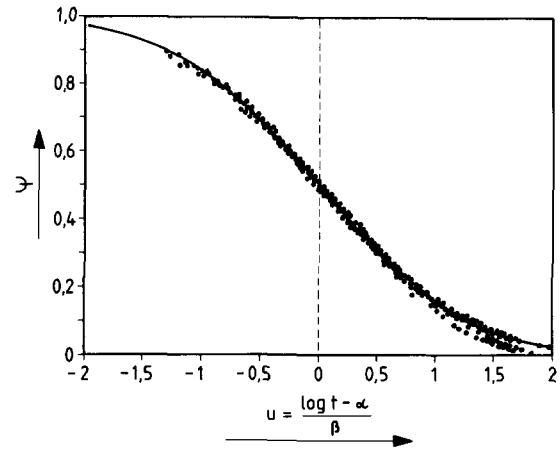

Figure 8 Data for the relaxation function Ψ *versus* the standardized time parameter $u = (\log t - \alpha)/\beta$ for indium, cadmium, lead, Lipowitz alloy, rubber hydrochloride, polyisobutylene, polyethylene and cetyl alcohol. The results are derived from Kubat's stress relaxation data[25,26] by applying the TC model with the CLND function under the restriction of $\beta = 1.9_0$. The full curve is the theoretical relaxation function

Table 2 Results for fitting the TC model to Kubat's data for the relaxation stress of a variety of materials[25,26]. The start values are the characteristic data given by Kubat

	Start values			Optimization results			
Material	$\sigma(0)$ (MPa)	Δt (s)	$\sigma_\infty/\sigma(0)$	$\sigma_0/\sigma(0)$	$\sigma_\infty/\sigma(0)$	α	r^2
In	2.0	6.2	0	1.27	0	1.10	0.986
Cd	13	1.7	0.1	1	0.03	2.58	>0.999
Pb	4.0	4.1	0.15	1	0.11	3.23	0.987
LA	380	1.5	0	1.11	0.01	1.48	>0.999
Rub-HCl	1.1	2×10^{-3}	0.32	1.12	0.31	−0.03	>0.999
PIB	0.04	6.2	0	1.18	0	2.46	0.986
PE	0.19	1.7	0.39	1.06	0.35	1.77	>0.999
Cet.alc.	0.4	1.2	0	1.16	0.04	1.11	0.999

In = indium, Cd = cadmium, Pb = lead, LA = Lipowitz alloy, Rub-HCl = rubber hydrochloride, PIB = polyisobutylene, PE = polyethylene, Cet.alc. = cetyl alcohol

during straining without undue reduction of the data range. It is hence not surprising that the ratio between the result of this analysis and Kubat's estimate is highest for indium, $\sigma_0/\sigma(0)=1.27$, where the separation of straining time and mean relaxation time on the log(time) scale is by far the smallest, namely $(\alpha-\log\Delta t)=0.31$, while for the other materials $\sigma_0/\sigma(0)$ is generally well below 1.2. The agreement between the estimates for $\sigma_\infty/\sigma(0)$ of Kubat and of this analysis is considered to be very satisfactory.

The broken curve in *Figure 7* marks the cases where for the relaxation function of a Nomex fibre $\beta=1.9_0$ is found in the optimization. The curve cuts through the surface such that it shows a well defined minimum with a value of $(1-r^2)\times10^4\simeq20$, which is marked (×) on the curve. On the basis of the preset standard deviation, the TC model described by equations (6) and (7) could in all cases be stably fitted to the data, applying the weighted linear regression procedure described in the Appendix.

DATA ANALYSIS AND RESULTS

The application of the TC model reveals the fine structure of $\Psi(\log t)$ as a function of strain. *Figures 9–11* summarize results for the relaxation curves of the materials at various strain levels, chosen to cover the individual experimental ranges.

For Nomex at low strains, up to the expected limit of the range of linear viscoelasticity of about 0.5–1%[2], the data follow the upper part of the S-shaped relaxation function, close to the upper limiting modulus. In *Figure 9* data are given for various low strains to illustrate the reproducibility of the measurements. The upper full curve is the theoretical relaxation function related to the experiment at 0.21% strain (marked by crosses). The coincidence of the data shows that, with respect to the relaxation function, Nomex fibres can be considered as being linear viscoelastic for strains up to ca. 1%. Going to higher strains around and beyond the yield point positions the data on the lower part of the relaxation function approaching the lower limiting modulus. The full curves, again, give the theoretical relaxation functions. The similarity of the curves for higher strains indicates a certain invariance of the viscoelastic properties of Nomex, as far as the relaxation function is concerned, once the yield region is reached.

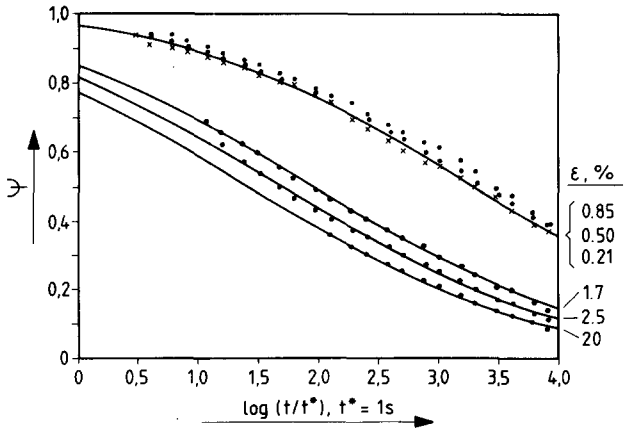

Figure 9 Relaxation function data for Nomex fibres at various strains as indicated. The full curve through the upper set of data points is the theoretical function for the data at 0.21% strain (×)

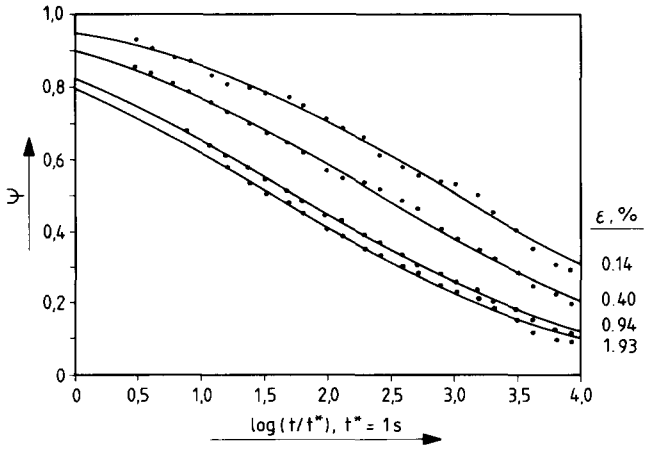

Figure 10 Relaxation function data and theoretical descriptions (full curves) for Kevlar fibre relaxation at various strains, as indicated

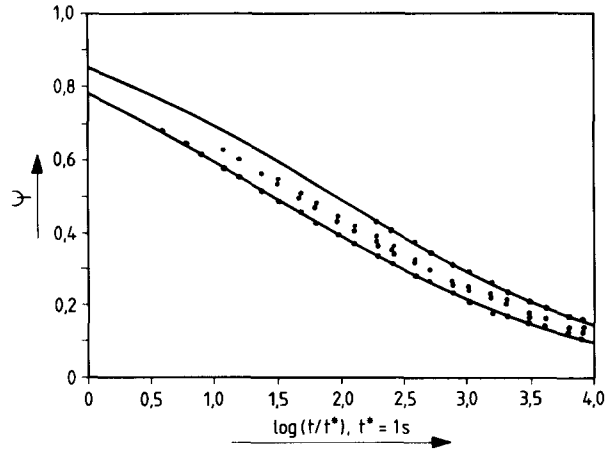

Figure 11 Relaxation function data for polypropylene fibre relaxation at strains between 0.33% and 58%. Full curves are theoretical descriptions for 0.33% (lower curve) and 30% strain (upper curve)

The situation is rather different for Kevlar fibres as illustrated in *Figure 10*. Again, for very low strains the data cover the upper part of the relaxation function without any strain range, however, where the curves would superimpose to indicate LVE behaviour. Increasing the strain seems to shift the data continuously on the theoretical relaxation function towards the lower part and already strains of 2% seem to suffice to approach the range of the lower limit of $\Psi(t)$.

Figure 11 summarizes results for the relaxation function for polypropylene fibres for strains between 0.33% and 58%. All data cover the lower part of the relaxation function that is shown for the two limiting cases of 0.33% and 30% strain, and show a great similarity. The shift to longer times that seems to suggest itself for higher strains is due to experimental scatter, so that in reality the curves show a coincidence over this extended strain range that is similar to the LVE performance of Nomex in the low-strain range. Such an extended LVE strain range is typical for amorphous polymers above their glass transition temperature[2].

Figure 12 summarizes the values for the log mean relaxation times for the three materials. The data relating to a given fibre type were shifted vertically for reasons of clarity. Again, three principally different types of behaviour are observed.

For Nomex the mean of the CLND function stays constant at low strains and shows a pronounced shift by

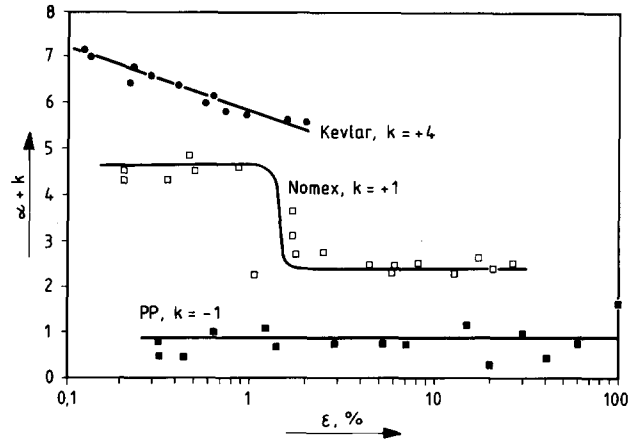

Figure 12 Log mean relaxation times vs. log strain for the three types of fibres. The data groups were shifted vertically for reasons of clarity by a factor of k, as given on the graph

ca. 2 decades in the range of 1.5–2% strain from $\alpha = 3.5_5 \pm 0.19$ (95% conf.limits, $\varepsilon < 1\%$) to $\alpha = 1.4_7 \pm 0.09$ for strains beyond 4%. The constancy of α for low and high strains corresponds to the invariance of the course of $\Psi(\log t)$, as shown in *Figure 9*.

In contrast to Nomex, where α stays constant for strains below ca. 1.5%, α drops for Kevlar already for the small-strain range, that is experimentally accessible, from a similar initial level as in Nomex, $\alpha(0.3\%) \simeq 3$, linearly with log strain by 1.5 orders of magnitude. This compares in size to the overall effect for Nomex ($0.2\% < \varepsilon < 30\%$).

For polypropylene the position of the CLND function on the log(time) scale turns out to be strain-invariant at a level of $\alpha = 1.7_8 \pm 0.18$ (95% conf.limits, $0.3\% < \varepsilon < 100\%$), which is in good agreement with the α values for Nomex at high strain levels. This observation is consistent with the theory that the yield of polymers reflects a solid–fluid transition[22,23]. Such a transition is observed for Nomex, which is well below T_g at room temperature (RT), while it is absent for PP, which at RT is well above T_g. The relation of the relaxation times to the transition temperatures and to the viscosity of the viscous component will be discussed in detail in part 2[4].

However, the change of the mean relaxation time is only one parameter to describe the relaxation performance. *Figures 13–15* summarize the changes of σ_0 and σ_∞ relative to $\sigma(0)$ with strain. Again, three distinctly different types of behaviour are observed.

Though the stress–strain curves of Nomex and Kevlar, given as $\sigma(0)$ *versus* ε in *Figures 13* and *14*, are quite different, the relaxation during straining is negligible in both cases, as expressed by the fact that σ_0 is equal to $\sigma(0)$, i.e. $\sigma_0/\sigma(0) = 1$, over the rather different strain ranges for both materials. This can be attributed to the considerable relaxation times still involved even at higher strains ($10^{1.5} \simeq 30$ s) and to the high relative contributions of the non-relaxing elastic component. For polypropylene the estimate for the true initial stress is 15% higher than the experimental initial stress, $\sigma_0/\sigma(0) = 1.14 \pm 0.06$ (95% conf. limits), which on the basis of similar mean relaxation times as in Nomex at higher strains can be attributed to the comparatively low relative contribution of the elastic component.

Figures 13–15 show that the elastic contributions to the initial stress show pronounced non-linearities with strain, reaching minima for Nomex, Kevlar and PP at strains of ca. 2%, 0.4% and 20–30%, respectively, which, for Nomex and polypropylene, agree well with the yield points of the materials. The specific consequences of these

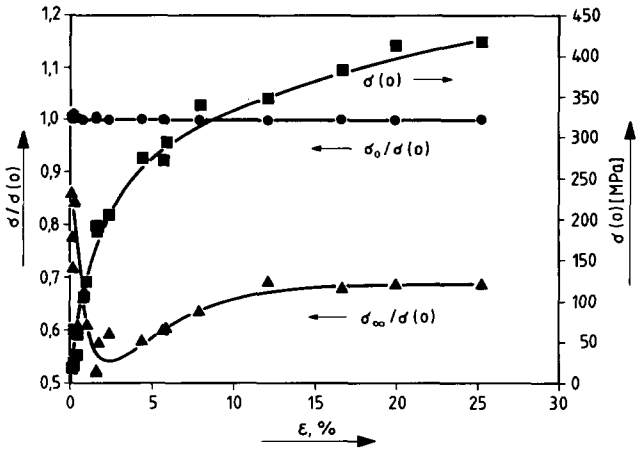

Figure 13 Experimental initial stress $\sigma(0)$ and relative values for the upper level (true initial) stress $\sigma_0/\sigma(0)$ and for the equilibrium stress $\sigma_\infty/\sigma(0)$ vs. strain obtained from fitting the TC model to the relaxation data for Nomex fibres

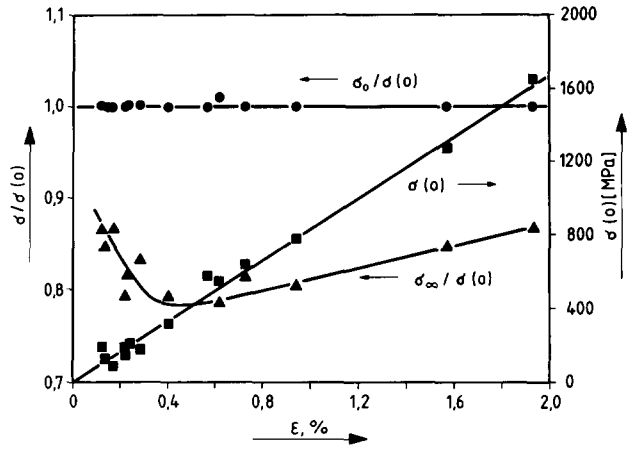

Figure 14 Experimental initial stress $\sigma(0)$ and the relative values for the upper level (true initial) stress $\sigma_0/\sigma(0)$ and for the equilibrium stress $\sigma_\infty/\sigma(0)$ vs. strain obtained from fitting the TC model to the relaxation data for Kevlar fibres

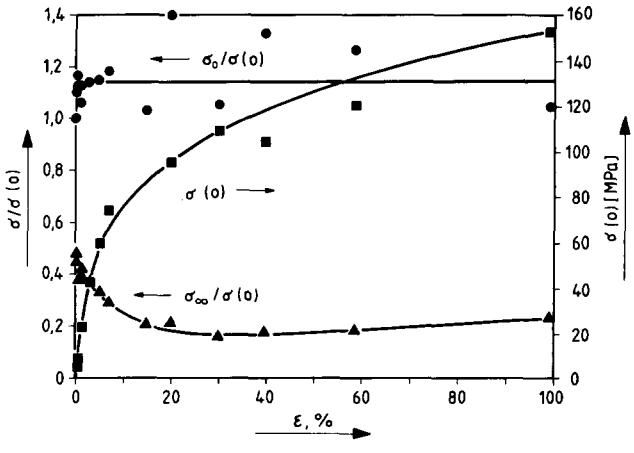

Figure 15 Experimental initial stress $\sigma(0)$ and the relative values for the upper level (true initial) stress $\sigma_0/\sigma(0)$ and for the equilibrium stress $\sigma_\infty/\sigma(0)$ vs. strain obtained from fitting the TC model to the relaxation data for polypropylene fibres

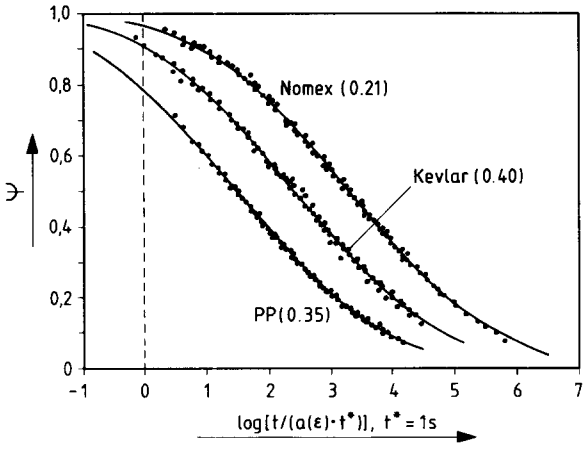

Figure 16 Values for the relaxation function derived from experimental data for the three types of fibres superimposed to form master curves for the reference strain as given in parentheses on the graph. $a(\varepsilon)$ is the acceleration factor given by equation (8)

non-linearities for the assessment of the limits of the strain range of linear viscoelasticity and for the determination of the strain-induced changes of the component moduli of the TC model as well as for their relation to fibre morphology are discussed in detail in part 2[4] of this work.

CONCLUSION

The analysis of the relaxation curves for the three different materials shows that the data can in all cases be successfully and consistently systematized on the basis of the TC model. The model contains the CLND function as a relaxation function, where the shape is assumed to be strain-invariant. The analysis of Kubat's data[25,26] for various materials rationalizes the *a priori* choice of the shape of the relaxation, given by the standard deviation, $\beta = 1.9_0$.

In this context it is important to note that the known shape of the relaxation function and its material invariance enables the determination of E_0 and/or E_∞ for a material even if only a relatively short part of the relaxation curve is experimentally accessible[27]. In this the TC model goes well beyond the possibilities of, for example, the Li-plot procedure to determine the elastic contribution to the material modulus[28,29].

The success of a superposition principle is generally judged by the quality of the master curve that may be generated for a chosen reference state. *Figure 16* summarizes the data from *Figures 9–11* in the form of such master curves for the reference strains given on the graph. The results of the procedure show a very satisfactory superposition of the data for the various strain ranges and a good fit by the CLND function, validating specifically the assumption of strain invariance of the shape of the relaxation function. The quality of the master curves gives weight to the validity of equation (7) to systematize the NLVE behaviour of the three different types of fibre materials. The implications of the primary results of the analysis are presented and discussed in detail in part 2 of this work[4].

ACKNOWLEDGEMENTS

The authors gratefully acknowledge the financial support of this investigation by the Deutsche Forschungsgemeinschaft (DFG) within the framework of the Sonderforschungsbereich 332, and also by the Ministerium für Wissenschaft und Forschung des Landes Nordrhein-Westfalen.

REFERENCES

1 Schapery, R. A. in 'Composite Materials', Vol. 2, 'Mechanics of Composite Materials' (Ed. G. P. Sendeckyi), Academic Press, New York, 1974, p. 85
2 Yannas, I. V. *J. Polym. Sci., Macromol. Rev.* 1974, **9**, 163
3 Menges, G. 'Werkstoffkunde der Kunststoffe', 2nd Edn., Hanser Verlag, München, 1984
4 Wortmann, F.-J. and Schulz, K. V. *Polymer* submitted
5 Ferry, J. D. 'Viscoelastic Properties of Polymers', 2nd Edn., Wiley, New York, 1970
6 Preston, P. *Encycl. Polym. Sci. Eng.* 1985, **11**, 381
7 Tashiro, K., Kobayashi, M. and Tadokoro, H. *Macromolecules* 1977, **10**, 413
8 Quirk, R. P. and Alsamarraie, M. A. A. in 'Polymer Handbook', 3rd Edn. (Eds. J. Brandrup and E. H. Immergut), Wiley, New York, 1989, p. V/27
9 Wortmann, F.-J. and Schulz, K. V. *Macromol. Chem., Macromol. Symp.* 1991, **50**, 55
10 Schulz, K. V. Diplomarbeit, RWTH Aachen, 1987
11 ASTM D2101-82, Annu.Book ASTM Standards 07.02 'Textiles—Fibers, Zippers', ASTM, Philadelphia, 1984
12 Alfrey, T. and Doty, P. *J. Appl. Phys.* 1945, **16**, 700
13 Feltham, P. *Br. J. Appl. Phys.* 1955, **6**, 26
14 Wiechert, E. *Wied. Ann. Physik Leipzig* 1893, **50**, 335, 546
15 Wortmann, F.-J. and DeJong, S. *Text. Res. J. 1985*, **55**, 750
16 Schulz, K. V., Wortmann, F.-J. and Höcker, H. *Wissenschaftl. Z. TH-Leuna Merseburg* 1991, **33**, 327
17 Wortmann, F.-J. and DeJong, S. *J. Appl. Polym. Sci.* 1985, **30**, 2195
18 Struik, L. C. E. 'Physical Ageing in Amorphous Polymers and Other Materials', Elsevier, Amsterdam, 1978
19 Schapery, R. A. *Polym. Eng. Sci.* 1969, **9**, 295
20 Matsuoka, S. in 'Failure of Plastics' (Eds. W. Brostow and R. D. Corneliussen), Hanser, Munich, 1986, p. 24
21 Yee, A. F., Bankert, R. J., Ngai, K. L. and Rendell, R. W. *J. Polym. Sci. (B) Polym. Phys.* 1988, **26**, 2463
22 Shay, R. M. and Caruthers, J. M. *J. Rheol.* 1986, **30**, 781
23 Nanzai, Y. *J. Non-Cryst. Solids* 1991, **131–133**, 516
24 Schulz, K. V. PhD Thesis, RWTH Aachen, 1990
25 Kubat, J. *Nature* 1965, **205**, 378
26 Kubat, J. 'A Similarity in the Stress Relaxation Behaviour of High Polymers and Metals', Acoprint, Stockholm, 1965
27 Wortmann, F.-J. Proc. 7th Int. Wool Text. Res. Conf., Tokyo, 1985, Vol. 1, p. 303
28 Li, J. C. M. *Can. J. Phys.* 1967, **45**, 493
29 Ek, C.-G., Kubat, J. and Rigdahl, M. *Colloid Polym. Sci.* 1987, **265**, 803
30 Henning, H.-J. and Wilrich, P.-Th. 'Statistische Methoden bei textilen Untersuchungen', Springer-Verlag, Berlin, 1974
31 Wilrich, P. Th. and Henning, H.-J. 'Formeln und Tabellen der angewandten, mathematischen Statistik', Springer-Verlag, Berlin, 1987
32 Hastings, C., Jr 'Approximations for Digital Computers', Princeton University Press, Princeton, NJ, 1955
33 Christian, S. D. and Tucker, E. E. *Int. Lab.* 1984, **16**(3), 10–18
34 Deming, W. E. 'Statistical Adjustment of Data', Dover, New York, 1964

APPENDIX

Applying the TC model as expressed in equation (3) yields for the values of the relaxation function Ψ:

$$\Psi(t) = [F(t) - F_\infty]/(F_0 - F_\infty) \qquad \text{(A1)}$$

where $F(t)$ is the experimentally determined force value, F_∞ the limiting equilibrium force to be approached in an individual experiment, and F_0 similarly the limiting initial force. Equivalent expressions may be obtained based on relative force, $F(t)/F(0)$, relaxation stress, $\sigma(t)$, or modulus, $E(t)$.

The fit of the cumulative log-normal distribution (CLND) function is based on a linearization of equation (6). To achieve this, the principles of the graphical method using cumulative probability paper[30] are applied, where $\Psi(t)$ is equated to $\Phi(u)$ of the standardized, cumulative normal distribution as:

$$\Psi(t)=\Phi(u)=(1/\sqrt{2\pi})\int_u^\infty \exp(-\tfrac{1}{2}u^2)\,dx \qquad (A2)$$

The related values of $u(\Phi)$ for the range $0<\Phi(u)\leqslant 0.5$ are given numerically by[31,32]:

$$u(\Phi)\simeq\eta-(a_0+a_1\eta+a_2\eta^2)/(1+b_1\eta+b_2\eta^2+b_2\eta^3) \qquad (A2)$$

with

$$\eta=\sqrt{\ln(1/\Phi^2)} \qquad (A4)$$

and

$$a_0=2.515517 \qquad b_1=1.432788$$
$$a_1=0.802853 \qquad b_2=0.189269$$
$$a_2=0.010328 \qquad b_3=0.001308$$

and with:

$$u(\Phi)=-u(1-\Phi) \qquad \text{for } 0.5<\Phi(u)<1 \qquad (A5)$$

The absolute error of the approximation is smaller than 4.5×10^{-4} in the range of $-3\leqslant u(\Phi)\leqslant+3$.

The plot of $u(\Phi)$ *versus* $\log t$ yields data points to which a straight line can be fitted by means of weighted linear regression. From the slope, b, and the intercept, a, of the line, the value for the mean α, and the standard deviation, β, are calculated:

$$\alpha=-a/b \qquad \beta=\alpha-(1-a)/b \qquad (A6)$$

With the knowledge of α and β the values for $\Psi(t)$ and $\Phi(u)$ corresponding to $u(t)$ are given numerically by[31,32]:

$$\Psi(t)\simeq\exp(2y)/[1+\exp(2y)]=\tfrac{1}{2}[1+\tanh(y)] \qquad (A7)$$

with

$$y=\sqrt{(2/\pi)}u(t)[1+0.044715\,u(t)^2] \qquad (A8)$$

The absolute error for $\Psi(t)$ after successive transformations according to equations (A3)/(A4) and (A7)/(A8) is limited to less than 1.8×10^{-4} for a range of $1.35\times10^{-3}\leqslant\Psi(t)\leqslant(1-1.35\times10^{-3})$ equivalent to the range of $-3\leqslant u\leqslant+3$.

The linearization of the CLND function via equations (A2)–(A4) imposes severe transformations onto the experimental values and their measurement errors, which require the application of appropriate weights in the linear regression procedure.

The straight line is fitted to the transformed set of data $[f(t),f(\Psi)]=[\log t,u(\Psi)]$ using the method of least squares, which aims at minimizing the function[33,34]:

$$S=\sum_{i=1}^{N} w_i[f(\Psi_i)-g(f(t_i))]^2 \qquad (A9)$$

where w_i are the weighting factors or weights, and $[f(\Psi_i)-g(f(t_i))]$ are termed residuals.

The method implies, justifiably, that $f(t_i)=\log(t_i)$ as the independent variable is measured with sufficient accuracy compared to Ψ_i to neglect its experimental error. The weights w_i are hence only functions of the uncertainty of $f(\Psi_i)$.

The selection of the weights is directed by the principle outlined by Deming[34], namely that w_i should be proportional to the inverse of the variance of the residual of the ith data set, which is identical to the variance of $f(\Psi_i)$, so that[33]:

$$S=\sum_{i=1}^{N}[f(\Psi_i)-g(f(t_i))]^2/\sigma^2_{f(\Psi_i)} \qquad (A10)$$

where the variance of the transformed experimental value $\sigma^2_{f(\Psi_i)}$ is given by applying the principles of error propagation as:

$$\sigma^2_{f(\Psi)}=[\delta f(\Psi)/\delta\Psi]^2\sigma^2_\Psi \qquad (A11)$$

so that:

$$1/\sigma^2_{f(\Psi)}=[\delta\Psi/\delta u(\Psi)]^2\,1/\sigma^2_\Psi \qquad (A12)$$

where:

$$\delta\Psi/\delta u=\psi(u) \qquad (A13)$$

$\psi(u)$ is the standardized log-normal distribution underlying the CLND function given by:

$$\psi(u)=(1/\sqrt{2\pi})\exp(-\tfrac{1}{2}u^2) \qquad (A14)$$

Assuming the measurement errors of Ψ_i as being constant over the whole measurement range, the individual weights w_i for the linearization of the CLND function, omitting constant factors, are taken as:

$$w_i=2\pi\psi(u_i)^2=\exp(-u_i^2) \qquad (A15)$$

Figure 17 shows the course of the weighting function plotted *versus* Ψ, indicating that attaching equal weights to all data points would be expected to lead to quite unreasonable results. The function rather gives differences of two orders of magnitude for the weights to be attached to feasible experimental readings of $\Psi=0.98$ or $\Psi=(1-0.98)$ compared to a reading at the inflection point of the relaxation function where $\Psi=0.5$. In the calculation procedure for linear regression the weight of an experimental value is introduced as would be the number of measurements in the case of multiple determinations with identical values.

The weighted linear regression is the basis for an optimization procedure, with the restriction of $\beta=1.9_0$, in which the initial and equilibrium values for force, stress or modulus, e.g. F_0 and F_∞, are chosen such that the coefficient of determination r^2 and hence the correlation coefficient r reach maxima and the coefficient of non-determination $(1-r^2)$ a minimum, respectively. All calculations were realized in a spreadsheet application on the basis of Quattro Pro (Borland).

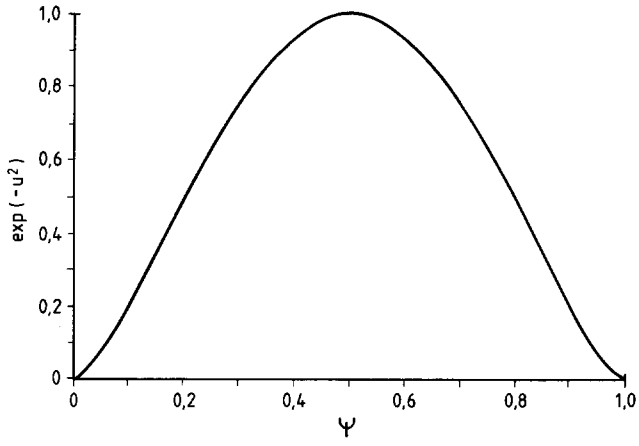

Figure 17 Weighting factors for fitting the CLND function to transformed experimental data for the relaxation function, using linear regression